

Room Temperature Mechanical Behavior of Monel K500 Alloy Fabricated via L-PBF and LP-DED

Indrajit Nandi^{1,2}, Paul R. Gradl³, Colton Katsarelis⁴, Shuai Shao^{1,2}, Nima Shamsaei^{1,2*}

¹National Center for Additive Manufacturing Excellence (NCAME), Auburn University, Auburn, AL 36849, USA

²Department of Mechanical Engineering, Auburn University, Auburn, AL 36849, USA

³Propulsion Department, NASA Marshall Space Flight Center, Huntsville, AL 35812, USA

⁴Materials and Failure Analysis, NASA Marshall Space Flight Center, Huntsville, AL 35812, USA

* Corresponding author:

Email: shamsaei@auburn.edu

Tel: (334) 844 4839

Abstract

This study investigated the room temperature mechanical behavior of Monel K500 fabricated using laser powder bed fusion (L-PBF) and laser powder directed energy deposition (LP-DED) technologies. The fabricated specimens underwent heat treatment involving hot isostatic pressing, solution annealing, and aging. The mechanical properties of the test specimens were evaluated using uniaxial tensile and fully reversed strain-controlled fatigue testing at room temperature. L-PBF specimens showed higher strength and lower ductility compared to the LP-DED counterparts. The LP-DED specimens showed longer fatigue life than the L-PBF specimens. The fracture surfaces were analyzed to investigate different crack initiation and failure mechanisms.

Keywords: Additive manufacturing; Laser powder bed fusion/fused (L-PBF); Laser powder directed energy deposition/deposited (LP-DED); Monel K500; Tensile; Fatigue

Introduction

Monel K500 (UNS N05500) is a γ' precipitation hardened Ni-base superalloy, and its major alloying element, copper (at ~30 wt.%), provides solid solution strengthening and improved corrosion resistance [1–3]. This alloy is particularly attractive for its high strength and hardness, and finds applications in offshore and marine industries [4]. Due to their high hardness, the conventional manufacturing and machining of Monel K500 alloy are often costly [5,6].

Additive manufacturing (AM) can be an attractive alternative for fabricating net-shaped Monel K500 parts with little to no machining at reduced time and material wastage, owing to its advantages of design flexibility and on-demand manufacturing [7,8]. Among different AM technologies, laser powder bed fusion (L-PBF) and laser powder directed energy deposition (LP-DED) are widely used [9–11]. Both processes fabricate parts in a layer-by-layer fashion, with L-PBF using scanning laser beams to selectively melt and fuse metal powder that is uniformly spread over a build plate, and LP-DED, which injects metal powder into a laser beam through a nozzle [12–14]. With AM being relatively new, the mechanical properties of additively manufactured (AM) Monel K500 parts have not been thoroughly investigated.

Due to the unique thermal characteristics of AM processes, such as rapid cooling and solidification, the AM microstructure in the non heat treated (NHT) condition is different from the wrought counterparts and often varies among different AM technologies due to their difference in thermal history [15–18]. Moreover, the presence of AM process-induced volumetric defects can be detrimental to the mechanical properties of AM parts [19,20]. This requires post-fabrication heat treatments (HT) to make the mechanical properties of AM parts comparable to their wrought counterparts [21–23]. This motivates investigating the effect of HT on the mechanical properties of L-PBF and LP-DED Monel K500. HT procedures involving hot isostatic pressing (HIP), solution annealing (SA), and aging were performed on the L-PBF and LP-DED Monel K500, and the effects on the tensile and fatigue behavior were investigated to evaluate the two AM technologies.

Experimental procedures

Vertical near net-shaped bars of 10 mm gage diameter and 80 mm length were fabricated by Quadrus Corporation using a Concept Laser M2 L-PBF machine. For LP-DED, cylindrical bars of 15 mm diameter and 100 mm length were fabricated by RPM Innovations (RPMI) Inc. using an RPMI 557 LP-DED machine. The chemical compositions of the powder batches used for the fabrication of L-PBF and LP-DED Monel K500 specimens are presented in Table 1 and the process parameters are listed in Table 2.

Table 1. Chemical compositions of the two Monel K500 powder batches, used to fabricate the L-PBF and LP-DED Monel K500 specimens.

Process	Elements	Cu	Al	Fe	Mn	Ti	Si	C	O	Ni
L-PBF	wt.%	28.4	2.88	0.43	0.75	0.60	<0.005	0.10	0.016	Bal.
LP-DED	wt.%	30	2.71	0.2	0.1	0.72	0.02	0.01	0.01	Bal.

Table 2. Process parameters used to fabricate the L-PBF and LP-DED Monel K500 specimens.

Process	Power (W)	Travel speed (mm/s)	Spot size (mm)	Hatch spacing (mm)	Layer thickness (mm)	Powder feed rate (g/min)	Process gas
L-PBF	152	600	0.120	0.105	0.030	---	Ar
LP-DED	1070	16.93	---	---	0.381	16.5	Ar

After fabrication, the L-PBF and LP-DED Monel K500 bars underwent HIP at 1163°C for 3 hours at a pressure of 100 MPa and furnace cooled to room temperature, followed by SA at 1100°C for 15 min, and argon quenched (AQ) to room temperature. Finally, the bars were aged at 610°C for 8 hr followed by AQ to room temperature.

Small coupons were excised from the NHT and heat treated (HT) Monel K500 bars. The coupons were mounted in epoxy and mirror polished. After polishing, the coupons were etched using Chromeregia reagent to reveal the microstructure on the radial, i.e., perpendicular to the build direction, and transverse planes, i.e., parallel to the build direction.

X-ray computed tomography (XCT) was performed on a coupon of 5 mm diameter and 5 mm height excised from the gauge section of the bars and investigated for volumetric defects. The XCT scans were performed using a Zeiss Xradia 620 Versa using a voltage of 150 kV and 23 W power, and a 5 μm voxel size. ImageJ and Dragonfly software were used to post-process the XCT scan for volumetric reconstruction and defect analysis.

The HT bars were machined to tensile and fatigue specimens (see Figure 1) according to the ASTM E8 and ASTM E606 standards, respectively [24,25]. Uniaxial tensile testing was performed at a strain rate of 0.005 mm/mm/min. An extensometer was attached to the specimens during the initial stage of tensile tests up to a strain value of 0.015 (mm/mm) to accurately measure the yield strength. Afterwards, it was removed due to the device's travel limit. Upon removal of the extensometer, the tests continued in force-controlled mode until fracture. Uniaxial fully reversed strain-controlled fatigue tests were performed on polished specimens at 0.005 mm/mm and 0.01 mm/mm strain amplitudes at room temperature. Following testing, the fracture surfaces of the tensile and fatigue specimens were investigated using a Zeiss Crossbeam 550 scanning electron microscope.

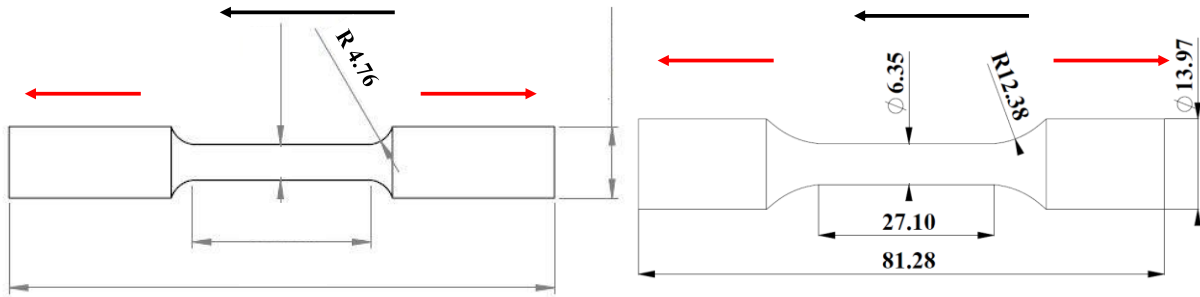


Figure 1. Geometries of the (a) tensile and (b) fatigue specimens used in this study (dimensions are in mm).

Results and discussion

The as-fabricated L-PBF and LP-DED bars contained more and larger defects within them. L-PBF bars showed larger defects and lower part density compared to LP-DED. HIP successfully closed the majority of the larger defects and increased the part density to a similar level for L-PBF and LP-DED Monel K500 (see Figure 2).

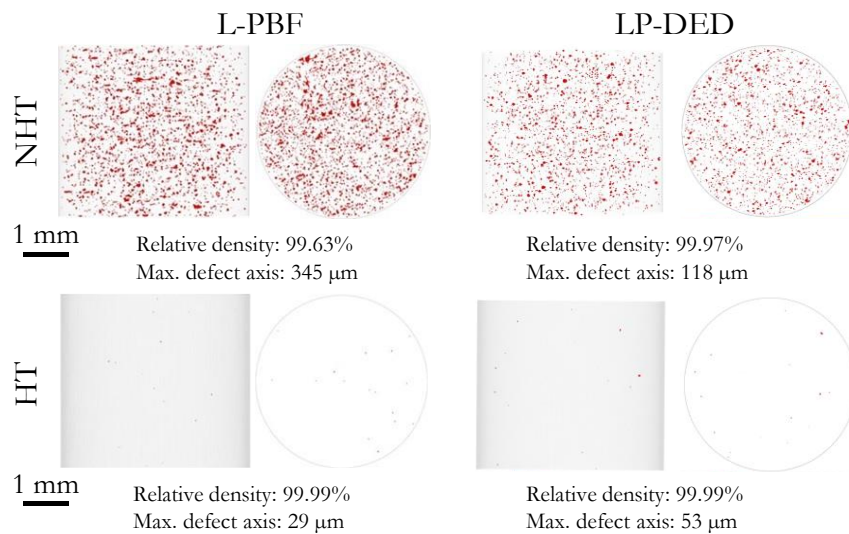


Figure 2. 3D XCT scan of L-PBF and LP-DED Monel K500 bars showing defects in NHT and HT conditions.

The microstructure of the NHT and HT L-PBF and LP-DED Monel K500 was examined (see Figure 3). The NHT condition showed long columnar grains in the longitudinal plane and distinct melt pool boundaries on the transverse plane. Following the HT, the microstructure was recrystallized. Melt pool and long columnar grains were no longer visible, and recrystallized grains with annealing twins were observed in both L-PBF and LP-DED Monel K500. Comparing the two different AM technologies, LP-DED exhibited larger grains, some on the order of 100 μm and above. While both LP-DED and L-PBF exhibited a combination of large and small grains, the grains in L-PBF were relatively smaller, primarily at and below 100 μm .

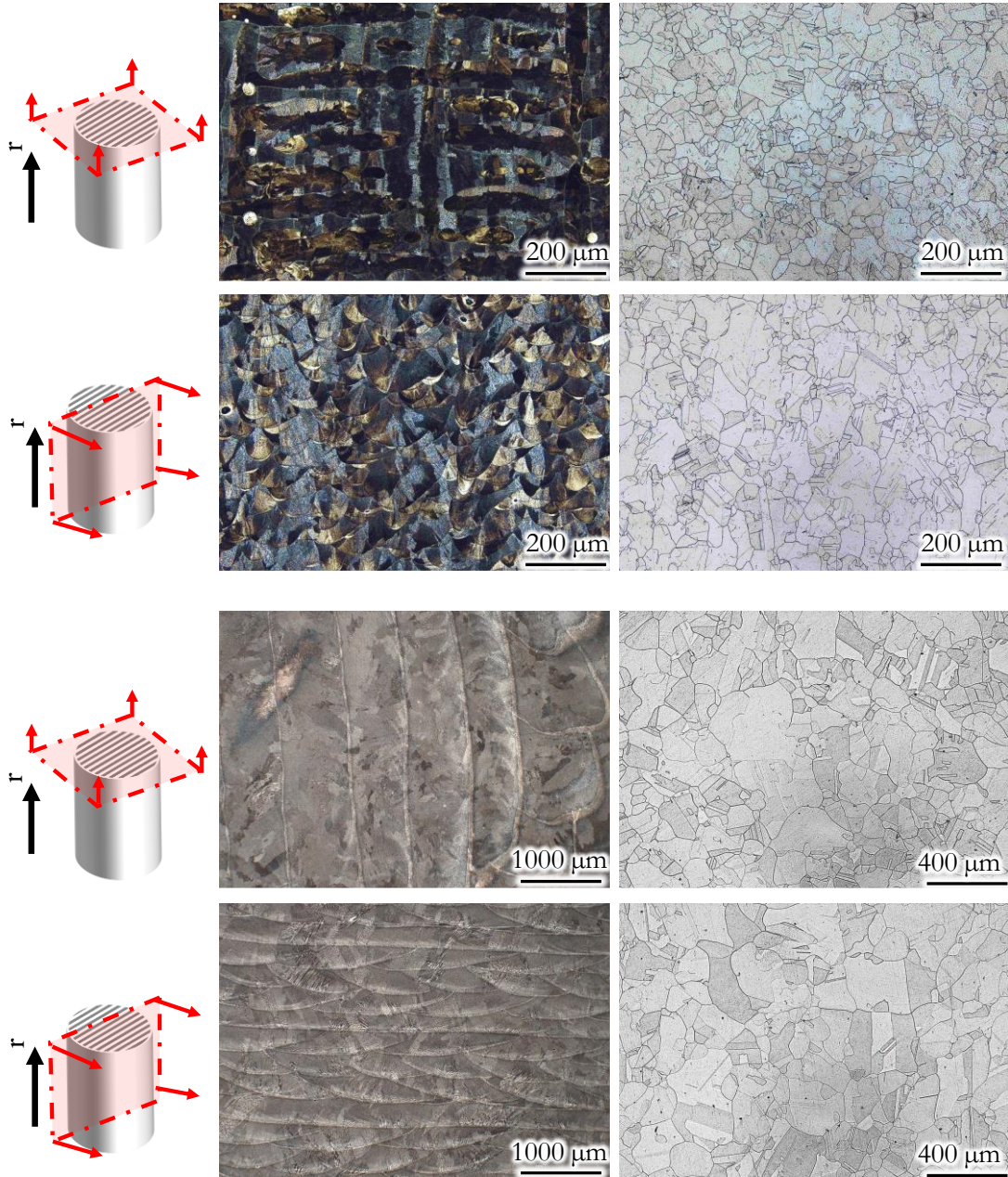


Figure 3. Etched micrograph of L-PBF and LP-DED Monel K500 showing variations in the grain structure in NHT and HT conditions.

The tensile properties, such as the ultimate tensile strength (UTS), yield strength (YS), and elongation at failure (%EL) for wrought, NHT L-PBF, and HT L-PBF and LP-DED Monel K500 are presented (see Figure 4a). HT resulted in an improved YS and UTS of L-PBF specimens, but a reduction in %EL compared to NHT. The LP-DED specimens showed lower YS and UTS than both NHT and HT L-PBF Monel K500 specimens but higher elongation than HT L-PBF Monel K500. Though HT improved the YS and UTS of L-PBF and LP-DED Monel

K500, their properties were lower than those of the wrought counterpart. Higher strength in L-PBF specimens was attributed to their finer grains present in the microstructure compared to LP-DED (see Figure 3). Both L-PBF and LP-DED tensile specimens showed ductile fracture with dimples present on the fracture surfaces (see Figure 4b). However, larger dimples were observed for the LP-DED specimens compared to the L-PBF counterparts. The higher elongation observed in the LP-DED specimens could be correlated with the coarser grain size.

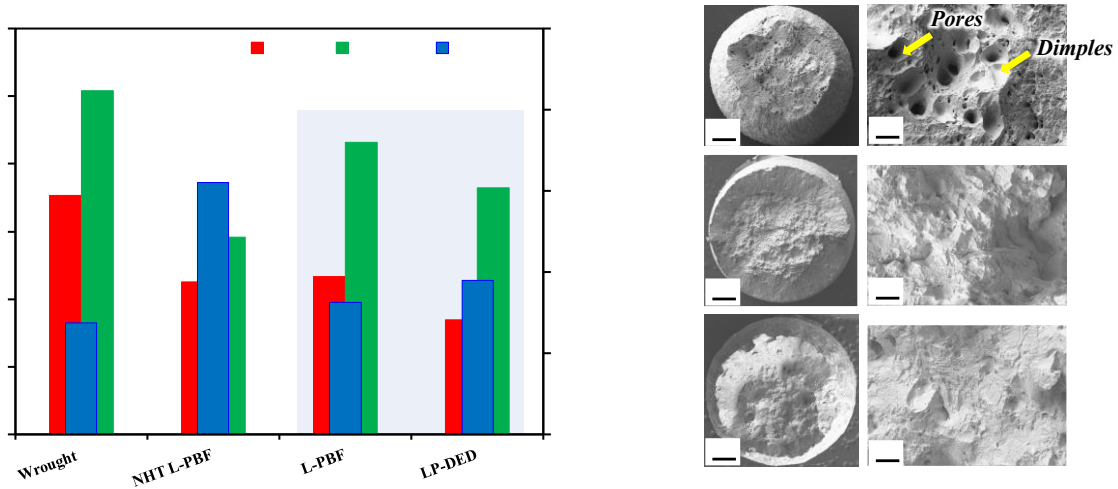


Figure 4. (a) Bar chart showing variations in tensile properties such as UTS, YS, and %EL of wrought, NHT L-L-PBF, HT L-PBF, and LP-DED Monel K500, and (b) tensile fracture surfaces.

The strain-life plot of HT L-PBF and LP-DED Monel K500 specimens is presented in Figure 5a. All specimens failed within the low to mid-cycle fatigue regime at both strain levels. LP-DED specimens showed longer fatigue life compared to the L-PBF ones, which was attributed to their coarser grains. As shown in Figure 5b, both L-PBF and LP-DED specimens showed microstructure mediated fatigue crack initiation instead of AM process induced volumetric defects. This was attributed to the HIP process eliminating the process induced volumetric defects from both L-PBF and LP-DED specimens (see Fig. 2). Crack propagated from those initiation sites, coalesced, and resulted in final failure. Larger grains in LP-DED specimens could reduce this crack propagation rate due to plasticity induced crack closure, resulting in longer fatigue life compared to L-PBF Monel K500 [18,26].

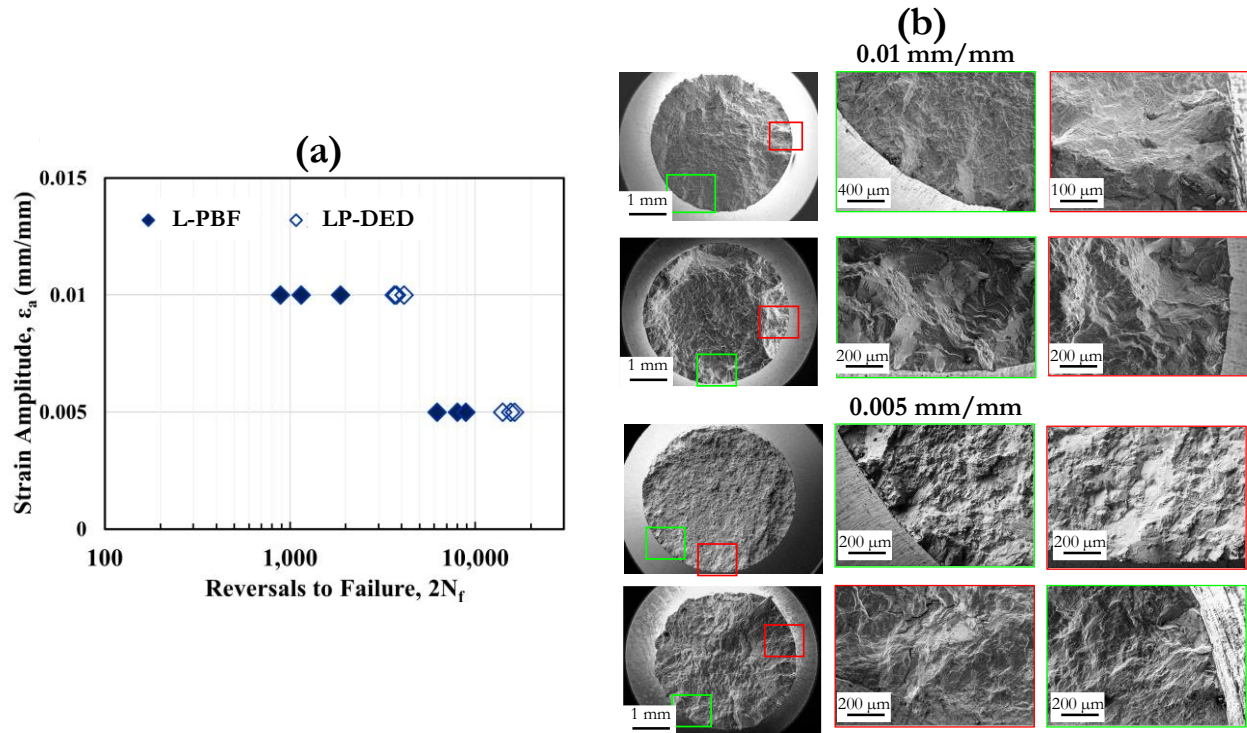


Figure 5. (a) Strain-life plot of L-PBF and LP-DED Monel K500 and (b) fatigue fracture surfaces.

Conclusions

In this study, the room temperature tensile and fatigue properties of laser powder bed fused (L-PBF) and laser powder directed energy deposited (LP-DED) Monel K500 were investigated. The following conclusions were drawn:

1. Hot isostatic pressing increased the part density by reducing the number of defects present in the fabricated L-PBF and LP-DED Monel K500 bars.
2. Heat treatment recrystallized the microstructure of L-PBF and LP-DED Monel K500, where the grain size was larger in LP-DED than in L-PBF.
3. L-PBF Monel k500 specimens showed higher strength and lower elongation compared to LP-DED ones, which was ascribed to the finer grain structure.
4. LP-DED specimens showed longer fatigue life compared to L-PBF specimens, which was attributed to their coarser grains.
5. Microstructure mediated fatigue crack initiation was observed for both LP-DED and L-PBF Monel K500 specimens.

Acknowledgment

This study is partially supported by the National Aeronautics and Space Administration (NASA) under contract No. 80MSFC19C0010 and the National Science Foundation (NSF) under grant No. 2319690. This paper describes objective technical results and analysis. Any subjective views or opinions that might be expressed in the paper do not necessarily represent the views of NASA, NSF, or the United States Government.

References

- [1] Chen Z, Wang C, Tang C, Lek YZ, Kandukuri SY, Du H, et al. Microstructure and mechanical properties of a Monel K-500 alloy fabricated by directed energy deposition. *Materials Science and Engineering: A* 2022;857:144113. <https://doi.org/10.1016/J.MSEA.2022.144113>.
- [2] Marenych O, Kostryzhev A, Shen C, Pan Z, Li H, van Duin S. Precipitation strengthening in Ni–Cu alloys fabricated using wire arc additive manufacturing technology. *Metals (Basel)* 2019;9. <https://doi.org/10.3390/met9010105>.
- [3] Kostryzhev AG, Marenych OO, Pan Z, Li H, van Duin S. Strengthening mechanisms in Monel K500 alloyed with Al and Ti. *J Mater Sci* 2023;58:4150–64. <https://doi.org/10.1007/S10853-023-08248-2>.
- [4] Megamex. Monel® K-500 2010:1–20.
- [5] Kulandaivel A, Kumar S. Effect of magneto rheological minimum quantity lubrication on machinability, wettability and tribological behavior in turning of Monel K500 alloy. <https://doi.org/10.10180/1091034420201765179>.
- [6] Esgin U, Özyürek D, Kaya H. An investigation of wear behaviors of different Monel alloys produced by powder metallurgy. *AIP Conf Proc* 2016;1727:16. <https://doi.org/10.1063/1.4945963/884222>.
- [7] Yadollahi A, Shamsaei N. Additive manufacturing of fatigue resistant materials: Challenges and opportunities. *Int J Fatigue* 2017;98:14–31. <https://doi.org/10.1016/J.IJFATIGUE.2017.01.001>.
- [8] Shamsaei N, Yadollahi A, Bian L, Thompson SM. An overview of Direct Laser Deposition for additive manufacturing; Part II: Mechanical behavior, process parameter optimization and control. *Addit Manuf* 2015;8:12–35. <https://doi.org/10.1016/J.ADDMA.2015.07.002>.
- [9] Gradl P, Mireles O, Andrews N. Introduction to Additive Manufacturing for Propulsion Systems. *Adv Mater Res* 2019;222:1–10.
- [10] Paul M, Soman S, Shao S, Shamsaei N. Fatigue crack growth in L-PBF Ti-6Al-4V: Influence of notch orientation, stress ratio, and volumetric defects. *Int J Fatigue* 2025;198:109027. <https://doi.org/10.1016/J.IJFATIGUE.2025.109027>.
- [11] Ahmad N, Bidar A, Ghiaasiaan R, Gradl PR, Shao S, Shamsaei N. A Comparison of Microstructure and Mechanical Performance of Inconel 718 Manufactured via L-PBF, LP-DED, and WAAM Technologies 2023. <https://doi.org/10.26153/TSW/50937>.
- [12] Dev Singh D, Mahender T, Raji Reddy A. Powder bed fusion process: A brief review. *Mater Today Proc* 2021;46:350–5. <https://doi.org/10.1016/J.MATPR.2020.08.415>.
- [13] Ahn DG. Directed Energy Deposition (DED) Process: State of the Art. *International Journal of Precision Engineering and Manufacturing-Green Technology* 2021 8:2 2021;8:703–42. <https://doi.org/10.1007/S40684-020-00302-7>.
- [14] Muhammad M, Gusain R, Ghiaasiaan SR, Gradl PR, Shao S, Shamsaei N. Microstructure and Mechanical Properties of Additively Manufactured Hayne 230: A comparative study of L-PBF vs. LP-DED. <http://dx.doi.org/10.26153/TSW/44174>.
- [15] Rahman MM, Huanes-Alvan G, Sahasrabudhe H, Chakrapani SK. Elastic Properties of IN718 Fabricated via Laser Directed Energy Deposition (DED). *Proceedings of 2021 48th Annual Review of Progress in Quantitative Nondestructive Evaluation, QNDE 2021* 2022. <https://doi.org/10.1115/QNDE2021-74848>.

- [16] Chakraborty S, Hebert D, Faisal TR. Variations of In-Plane Mechanical Properties of Cellular Structures With Different Hierarchical Organizations. ASME International Mechanical Engineering Congress and Exposition, Proceedings (IMECE) 2021;12. <https://doi.org/10.1115/IMECE2020-24050>.
- [17] Poudel B, Nguyen HX, Oneil A, Ahmad MU, Qu Z, Kwon P, et al. Selective Laser Melting and Mechanical Properties of Oxide Dispersion Strengthened Haynes 214 Alloy. Proceedings of ASME 2022 17th International Manufacturing Science and Engineering Conference, MSEC 2022 2022;2. <https://doi.org/10.1115/MSEC2022-85620>.
- [18] Paul M, Ghiaasiaan R, Gradl P, Caron J, Wang P, Shao S, et al. Tensile and fatigue behaviors of newly developed HAYNES® 233 alloy: Additively manufactured vs. wrought. Mater Des 2024;244:113165. <https://doi.org/10.1016/J.MATDES.2024.113165>.
- [19] du Plessis A, Yadroitsava I, Yadroitsev I. Effects of defects on mechanical properties in metal additive manufacturing: A review focusing on X-ray tomography insights. Mater Des 2020;187:108385. <https://doi.org/10.1016/J.MATDES.2019.108385>.
- [20] Wilson PJ, Azizian-Farsani E, Paul M, Khonsari MM, Shao S, Shamsaei N. On the damping and fatigue characterization of additively manufactured Ti-6Al-4V. Additive Manufacturing Letters 2024;11:100260. <https://doi.org/10.1016/J.ADDLET.2024.100260>.
- [21] Laleh M, Sadeghi E, Revilla RI, Chao Q, Haghdadi N, Hughes AE, et al. Heat treatment for metal additive manufacturing. Prog Mater Sci 2023;133:101051. <https://doi.org/10.1016/J.PMATSCI.2022.101051>.
- [22] Harris ZD, Burns JT. The effect of isothermal heat treatment on hydrogen environment-assisted cracking susceptibility in Monel K-500. Materials Science and Engineering: A 2019;764:138249. <https://doi.org/10.1016/J.MSEA.2019.138249>.
- [23] Khan MF, Ghiaasiaan R, Gradl PR, Shao S, Shamsaei N. Additively Manufactured Scalmalloy via Laser Powder Bed Fusion (L-PBF): Temperature-Dependent Tensile and Fatigue Behaviors. Fatigue Fract Eng Mater Struct 2025;48:1496–513. <https://doi.org/10.1111/FFE.14549>.
- [24] Committee, E08 AE. Standard Test Methods for Tension Testing of Metallic Materials. ASTM International; 2020.
- [25] Test Method for Strain-Controlled Fatigue Testing 2021. https://doi.org/10.1520/E0606_E0606M-21.
- [26] Muhammad M, Ghiaasiaan R, Gradl PR, Schobel A, Godfrey D, Shao S, et al. Temperature-dependent fatigue behavior of additively manufactured Hastelloy-X: The effect of manufacturing process. J Manuf Process 2025;136:123–36. <https://doi.org/10.1016/J.JMAPRO.2025.01.068>.